

Development of a beam-based phase feed-forward
demonstration at the CLIC Test Facility (CTF3).

Jack Roberts
New College, Oxford

Thesis submitted in fulfilment of the requirements for the degree of Doctor
of Philosophy at the University of Oxford

Trinity Term, 2016

Abstract

This is the abstract TeX for the thesis and the stand-alone abstract.

Dedication.

Acknowledgements

Acknowledgements.

Contents

| | | |
|----------|---|----------|
| 1 | Introduction | 1 |
| 1.1 | Particle Physics | 1 |
| 1.2 | Particle Colliders | 1 |
| 1.3 | Motivation for Future Linear Colliders | 1 |
| 1.4 | CLIC | 1 |
| 1.5 | FONT | 1 |
| 1.6 | Phase Feedforward for CLIC | 1 |
| 1.7 | Thesis Overview | 1 |
| 2 | Design of the PFF Prototype at CTF3 | 2 |
| 2.1 | CTF3 | 2 |
| 2.1.1 | Goals of CTF3 | 2 |
| 2.1.2 | Layout of CTF3 | 2 |
| 2.2 | Design of the PFF Prototype at CTF3 | 2 |
| 2.2.1 | Schematic Overview of PFF System | 2 |
| 2.2.2 | Latency | 3 |
| 2.3 | PFF Hardware | 3 |
| 2.3.1 | FONT5 Board | 3 |
| 2.3.2 | Amplifier | 3 |
| 2.3.3 | Phase Monitors | 3 |
| 2.3.4 | Kickers | 3 |
| 2.4 | Differences Between PFF at CTF and CLIC | 3 |
| 2.4.1 | Phase Sag | 3 |
| 2.4.2 | Pulse Length | 3 |
| 2.5 | Feedforward Algorithm | 3 |
| 2.5.1 | Theoretical Corrected Jitter | 3 |
| 2.5.2 | Theoretical Optimal Gain | 3 |
| 3 | Optics for the PFF Prototype | 4 |
| 3.1 | Introduction to Optics | 4 |
| 3.1.1 | MADX | 5 |
| 3.2 | TL2 | 5 |
| 3.2.1 | Lattice | 5 |
| 3.2.2 | Integration of PFF Hardware | 5 |
| 3.2.3 | Optics Constraints | 5 |
| 3.3 | TL2 Optics Measurements | 5 |

| | | |
|----------|---|-----------|
| 3.3.1 | Method | 5 |
| 3.3.2 | Results | 5 |
| 3.3.3 | Sources of Errors in MADX Model | 5 |
| 3.3.4 | Corrections to MADX Model | 5 |
| 3.4 | Matched TL2 Optics | 5 |
| 3.4.1 | MADX Optics Matching | 5 |
| 3.4.2 | Nominal Optics | 5 |
| 3.4.3 | PFF Optics | 5 |
| 4 | Phase Monitor Performance | 6 |
| 4.1 | Phase Monitor Electronics | 7 |
| 4.2 | Signal Response Measurements | 7 |
| 4.2.1 | Experimental Setup | 7 |
| 4.2.2 | Saturation | 7 |
| 4.2.3 | Cross-Talk | 7 |
| 4.3 | Calibrations | 7 |
| 4.3.1 | Procedure | 7 |
| 4.3.2 | Single Sample Results | 7 |
| 4.3.3 | Multi-Sample Results | 7 |
| 4.4 | Digitiser Noise | 7 |
| 4.4.1 | On FONT5 Board | 7 |
| 4.4.2 | On SiS Digitiser | 7 |
| 4.5 | Phase Shifter Noise | 7 |
| 4.5.1 | Digital Phase Shifters | 7 |
| 4.5.2 | Mechanical Phase Shifters | 7 |
| 4.6 | Resolution | 7 |
| 4.7 | Linearity | 10 |
| 4.8 | Bandwidth | 10 |
| 4.9 | Dependence on Position | 10 |
| 5 | Phase Propagation | 11 |
| 5.1 | Definitions of Different Phase Statistics | 11 |
| 5.2 | Characteristics of Uncorrected Phase Jitter | 11 |
| 5.3 | First Order Energy Dependencies | 11 |
| 5.3.1 | Correlation between Phase and Energy | 11 |
| 5.3.2 | R56 | 11 |
| 5.3.3 | Effect of R56 in TL2 | 14 |
| 5.4 | Mitigation of First Order Energy Dependence | 18 |
| 5.4.1 | Matched Optics for TL1 | 21 |
| 5.4.2 | Scans of R56 in TL1 | 23 |
| 5.5 | Higher Order Energy Dependencies | 30 |
| 5.5.1 | Expected Dependence due to Optics | 30 |
| 5.5.2 | Energy Variation Along the Pulse | 31 |
| 5.5.3 | R56 Scans whilst Varying Beam Energy | 31 |
| 5.5.4 | Mitigation of Higher Order Dependencies | 35 |

| | | |
|----------|---|-----------|
| 5.5.5 | Effect on PFF Operation | 35 |
| 5.6 | Other Sources of Phase Jitter | 35 |
| 5.6.1 | Combiner Ring Septum | 35 |
| 5.6.2 | TL1 & Combiner Ring Bends | 35 |
| 5.7 | Best Phase Propagation | 35 |
| 6 | Setup and Commissioning of the PFF System | 36 |
| 6.1 | Feedforward Controller (FONT5a Board) | 36 |
| 6.1.1 | Installation | 36 |
| 6.1.2 | Setup Parameters and DAQ | 36 |
| 6.1.3 | ADC Droop Correction | 41 |
| 6.1.4 | Implementation of PFF Algorithm in Firmware | 46 |
| 6.2 | Amplifier | 49 |
| 6.2.1 | Installation | 50 |
| 6.2.2 | Linearity | 52 |
| 6.2.3 | Shape | 55 |
| 6.2.4 | Bandwidth | 57 |
| 6.3 | Data Acquisition and Signal Processing | 58 |
| 6.3.1 | SiS Digitiser Setup | 58 |
| 6.3.2 | Acquisition Tools | 58 |
| 6.3.3 | Monitoring Tools | 58 |
| 6.3.4 | Time Alignment of Signals | 59 |
| 6.3.5 | Definition of Zero Phase | 59 |
| 6.4 | Kicker and Optics Performance Verification | 59 |
| 6.4.1 | Correction Range | 59 |
| 6.4.2 | Variations Along Pulse | 63 |
| 6.4.3 | Shape | 63 |
| 6.4.4 | Orbit Closure | 64 |
| 6.5 | Correction Output Timing | 67 |
| 6.5.1 | Kicker Cable Lengths | 69 |
| 6.5.2 | Absolute Timing | 71 |
| 6.5.3 | Relative Kicker Timing | 76 |
| 7 | Early Phase Feedforward Attempts and Simulations | 83 |
| 7.1 | Gain Scans | 83 |
| 7.2 | Simulation Method | 83 |
| 7.3 | Effect of Limited Correction Range | 83 |
| 7.4 | Effect of Timing Offsets | 83 |
| 7.5 | Effect of Limited Bandwidth | 83 |
| 7.6 | Effect of Variations Along the Pulse | 83 |
| 7.7 | Effect of Amplifier Non-linearities | 83 |
| 8 | Best Achieved Phase Stabilisation | 84 |
| 8.1 | Lowest Achieved Phase Jitter | 84 |
| 8.1.1 | Mean Phase Jitter | 85 |

| | | |
|-----------|---|------------|
| 8.1.2 | Correction of Pulse Shape | 87 |
| 8.1.3 | Phase Jitter Along the Pulse | 88 |
| 8.2 | Correction on Longer Time Scales | 89 |
| 8.2.1 | Upstream Phase Drifts | 93 |
| 8.2.2 | Gain Stability | 95 |
| 8.2.3 | Results | 98 |
| 8.3 | Possible Areas for Future Improvement | 101 |
| 9 | Alternative Phase Feedforward Setups and Complementary Systems | 107 |
| 9.1 | Correction with Additional Jitter Source | 107 |
| 9.2 | Slow Correction | 107 |
| 9.2.1 | Implementation | 108 |
| 9.2.2 | Results | 108 |
| 10 | Conclusions | 109 |
| 10.1 | Summary | 109 |
| 10.2 | Future Work | 109 |
| | Bibliography | 110 |

List of Figures

| | | |
|------|---|----|
| 2.1 | CTF3 schematic. | 2 |
| 3.1 | New TL2 lattice for PFF. Changes highlighted yellow. | 4 |
| 3.2 | Mean phase along. | 5 |
| 4.1 | Dig shifter 1. | 8 |
| 4.2 | Dig shifter 2. | 8 |
| 4.3 | Dig shifter 3. | 8 |
| 4.4 | Mech shifter. | 9 |
| 4.5 | Resolution. | 9 |
| 5.1 | Downstream phase jitter vs. residual R56 between monitors. | 15 |
| 5.2 | Phase correlation vs. residual R56 between monitors. | 16 |
| 5.3 | Phase correlation vs. residual R56 between monitors. | 17 |
| 5.4 | Phase correlation vs. residual R56 between monitors. | 18 |
| 5.5 | TL1 [REF]. | 20 |
| 5.6 | Matched R56 values for TL1. | 22 |
| 5.7 | Current vs. R56 for the CT.QFG0750 quadrupole in TL1. | 23 |
| 5.8 | Horizontal beta in TL1 for all R56 optics. | 24 |
| 5.9 | Vertical beta in TL1 for all R56 optics. | 25 |
| 5.10 | Dispersion in TL1 for all R56 optics. | 26 |
| 5.11 | Phase jitter during scan of R56 in TL1. | 27 |
| 5.12 | Correlation during scan of R56 in TL1. | 28 |
| 5.13 | Upstream and downstream beam conditions during the R56 scan. | 29 |
| 5.14 | Mean phase jitter during R56 scan 2. | 30 |
| 5.15 | Mean phase jitter during R56 scan 3. | 31 |
| 5.16 | Phase jitter for different R56 whilst wiggling gun current. | 32 |
| 5.17 | Phase vs. energy for different R56 in TL1. | 32 |
| 5.18 | Mean downstream phase along the pulse for different R56 values. | 33 |
| 5.19 | Mean downstream phase along the pulse for different R56 values. | 34 |
| 6.1 | Front panel of the FONT5a board. | 37 |
| 6.2 | Diode output along the pulse with the IIR filter off and on. | 38 |
| 6.3 | Diode output along the pulse with the IIR filter off and on. | 41 |
| 6.4 | Exponential fit to diode droop. | 42 |
| 6.5 | Residuals between diode exponential fit and actual diode output. | 43 |
| 6.6 | Diode output along the pulse with the IIR filter off and on. Zoomed in. . . . | 45 |

| | | |
|------|--|----|
| 6.7 | Phase along the pulse with the IIR filter off and on. | 45 |
| 6.8 | Difference between the phase reconstruction method used in the PFF algorithm on the FONT5a board (with the small angle approximation) and the full reconstruction used with data acquired from the SiS digitisers. | 48 |
| 6.9 | Achievable PFF jitter versus phase offset for full phase reconstruction and with the small angle approximation. | 49 |
| 6.10 | Front panel of the amplifier. | 50 |
| 6.11 | Cabling setup for cables between the amplifier and kickers. | 51 |
| 6.12 | Amplifier output vs. input. | 53 |
| 6.13 | Residual between amplifier output and linear fit. | 54 |
| 6.14 | Amp L along pulse at 1 V input | 55 |
| 6.15 | Amp R along pulse at 1 V input | 56 |
| 6.16 | Flatness of potential difference sent to kickers. | 57 |
| 6.17 | Residual kick along pulse. | 58 |
| 6.18 | Residual kick along pulse: deviation from flat. | 59 |
| 6.19 | Phase shift versus amplifier input voltage. | 60 |
| 6.20 | Phase shift versus amplifier input voltage. | 61 |
| 6.21 | Traces relative timing scan. | 63 |
| 6.22 | Traces relative timing scan. | 64 |
| 6.23 | Horizontal orbit offset in and around the TL2 chicane at different input voltages sent to the amplifier. | 65 |
| 6.24 | Orbit in the TL2 chicane at 1 V amplifier input for the BPM data, nominal model and model taking in to account the difference in amplifier output voltage to each kicker. | 66 |
| 6.25 | Orbit in the TL2 chicane at 1 V amplifier input for the BPM data, nominal model and model taking in to account the quadrupole currents in the real machine setup. | 68 |
| 6.26 | Beam pickup on kicker strips as seen on amplifier monitoring signals. | 72 |
| 6.27 | Output delay of 0 clock cycles. Full pulse. | 73 |
| 6.28 | Output delay scan, end of pulse. | 74 |
| 6.29 | Output delay of 7 clock cycles. Full pulse. | 75 |
| 6.30 | Output delay of 7 clock cycles. End of pulse. | 75 |
| 6.31 | Kick output with no delay as seen on BPM and phase signals. | 77 |
| 6.32 | Fit time offset between kick and beam at different output delays. | 78 |
| 6.33 | Alignment between BPMs and phase signals with optimal delay applied in analysis. | 79 |
| 6.34 | Simulated response to offset kicks. | 80 |
| 6.35 | Measured BPM offset for different relative kick delays. | 81 |
| 6.36 | Fitted peak BPM offset vs. relative kick delay. | 82 |
| 8.1 | Mean phase. | 85 |
| 8.2 | Simulated PFF. | 87 |
| 8.3 | Mean phase along. | 88 |
| 8.4 | Flatness. | 89 |
| 8.5 | Std phase along. | 90 |

| | | |
|------|---|-----|
| 8.6 | Std phase along. | 90 |
| 8.7 | History of mean phase across datasets. | 92 |
| 8.8 | History of mean phase across datasets, with mean subtraction. | 92 |
| 8.9 | Fraction of pulses outside the correction range along the pulse. [TODO: Add line using real dataset offsets] | 94 |
| 8.10 | Offset between downstream phase with FF off and FF on. | 95 |
| 8.11 | Upstream and downstream phase jitter in each data set. | 97 |
| 8.12 | Upstream-downstream mean phase correlation in each dataset with PFF off. | 97 |
| 8.13 | Correlation vs. phase jitter ratio. | 98 |
| 8.14 | Gain used in each dataset compared to the optimal gain. | 99 |
| 8.15 | Theoretical corrected downstream jitter with optimal and used gain. | 101 |
| 8.16 | Corrected downstream jitter with the actual PFF system. | 102 |
| 8.17 | Histogram showing overall distribution of downstream phase with FF off and on. | 103 |
| 8.18 | Downstream phase vs. upstream phase with FF off. | 104 |
| 8.19 | Downstream phase vs. upstream phase with FF on. | 104 |
| 8.20 | Downstream phase vs. upstream phase with FF simulated at optimal gain. | 105 |
| 8.21 | Downstream phase vs. upstream phase with FF simulated with actual gain used. | 105 |

List of Tables

| | | |
|-----|--|-----|
| 5.1 | Typical upstream phase and energy conditions at CTF3. | 14 |
| 5.2 | Initial and final conditions for optics matching in TL1. | 21 |
| 6.1 | IIR filter weights for the FONT5a board ADCs. | 44 |
| 6.2 | Feedforward results using combined data from 20th November 2015. | 54 |
| 6.3 | Phase shift at +1 volt input to the amplifier. | 60 |
| 6.4 | Lengths of cables between the amplifier and the patch panel. | 70 |
| 6.5 | Lengths of cables between the patch panel and the kickers. | 71 |
| 8.1 | Best PFF results. | 86 |
| 8.2 | Simulated feedforward results from 20th November 2015. | 102 |
| 8.3 | Feedforward results from 20th November 2015. | 103 |
| 8.4 | Feedforward results using combined data from 20th November 2015. [TODO: this table shows results from old simulations!] | 106 |

Glossary

Item1 Description.

Item2 Description.

Item3 Description.

Chapter 1

Phase Propagation

This is the introductory text.

1.1 Definitions of Different Phase Statistics

Definitions of different types of phase jitter.

1.2 Characteristics of Uncorrected Phase Jitter

Injector feedbacks etc.

1.3 First Order Energy Dependencies

1.3.1 Correlation between Phase and Energy

energy jitter

Upstream AND downstream

1.3.2 R56

Assuming energy is the only source of differences between the upstream and downstream phase, the downstream phase, ϕ_d , can be expressed in terms of the optics transfer matrix coefficient R_{56} (Section ??) as follows:

$$\phi_d = \phi_u + R_{56} \frac{\Delta p}{p} \tag{1.1}$$

Where ϕ_u is the upstream phase, $\Delta p/p$ is the relative energy offset and R_{56} is the R56 value between the upstream and downstream phase monitors, defined by the machine optics. R56 defines the phase shift between two points in the lattice resulting from a beam energy offset. The units of R56 in the equation above are 12 GHz radians per unit relative energy offset ($\Delta p/p = 1$). MADX uses units of metres and this value is what will be referred to in this chapter. To obtain the R56 value to use in the equation above the MADX value must be multiplied by the conversion factor $2\pi/0.025$, where 0.025 m is the 12 GHz wavelength.

In terms of jitters Equation 5.1 becomes:

$$\sigma_d = \sqrt{\sigma_u^2 + R_{56}^2 \sigma_p^2 + 2R_{56}\rho_{up}\sigma_u\sigma_p} \quad (1.2)$$

Where σ_d is the downstream phase jitter, σ_u is the upstream phase jitter, σ_p is the relative energy jitter and ρ_{up} is the correlation between the upstream phase and the energy. This follows from the result of adding correlated variances. Clearly, any non-zero R56 between the upstream and downstream phase monitors introduces an additional energy component to the downstream phase that increases the downstream phase jitter.

The effect of R56 on the upstream-downstream phase correlation, ρ_{ud} , can also be defined starting from the definition of the correlation coefficient:

$$\rho_{ud} = \frac{\text{cov}[\phi_u, \phi_d]}{\sigma_u \sigma_d} \quad (1.3)$$

Where $\text{cov}[\phi_u, \phi_d]$ is the covariance between the upstream and downstream phase, given by:

$$\text{cov}[\phi_u, \phi_d] = \frac{1}{N} \sum_{i=1}^N \phi_{ui} \phi_{di} \quad (1.4)$$

By inserting the definition of the downstream phase from Equation 5.1 and separating the terms in the sum this becomes:

$$\text{cov}[\phi_u, \phi_d] = \frac{1}{N} \sum_{i=1}^N \phi_{ui}^2 + R_{56} \frac{1}{N} \sum_{i=1}^N \phi_{ui} \frac{\Delta p}{p} \quad (1.5)$$

The first term is now the variance of the upstream phase, σ_u^2 , and the second term is R_{56} multiplied by the covariance between the upstream phase and the energy, $\text{cov}[\phi_u, \frac{\Delta p}{p}]$, which can be expressed in terms of the correlation between the upstream phase and the energy, ρ_{up} :

$$\text{cov}\left[\phi_u, \frac{\Delta p}{p}\right] = \rho_{up} \sigma_u \sigma_p \quad (1.6)$$

Therefore, Equation 5.5 becomes:

$$\text{cov}[\phi_u, \phi_d] = \sigma_u^2 + R_{56} \rho_{up} \sigma_u \sigma_p \quad (1.7)$$

Finally, substituting Equations 5.2 and 5.7 into Equation 5.3 gives:

$$\rho_{ud} = \frac{\sigma_u + R_{56} \rho_{up} \sigma_p}{\sqrt{\sigma_u^2 + R_{56}^2 \sigma_p^2 + 2R_{56} \rho_{up} \sigma_u \sigma_p}} \quad (1.8)$$

Considering that in this model the only difference between the upstream and downstream phase results from the R56, it is perhaps obvious that the best conditions for the PFF correction are obtained when the R56 coefficient between the upstream and downstream phase monitors is zero. In these conditions $\sigma_d = \sigma_u$ and $\rho_{ud} = 1$. This can be more formally defined by using the expression for the theoretical corrected downstream phase jitter when using the optimal gain factor as derived in Section 2.5.1:

$$\sigma_{PFF} = \sigma_d \sqrt{1 - \rho_{ud}^2} \quad (1.9)$$

All these quantities have been derived above and inserting them in to this equation gives the following expression for the corrected downstream phase jitter in terms of the R56:

$$\sigma_{PFF} = |R_{56}| \sigma_p \sqrt{1 - \rho_{up}^2} \quad (1.10)$$

As expected the achievable corrected downstream phase jitter is minimised when $R_{56} = 0$. Note that this equation does not take in to account the effects of the phase monitor resolution, which in reality limits the minimum achievable downstream phase jitter to $\sigma_{PFF} = 0.2^\circ$ ([TODO:Section ref]).

In principle the beam conditions for the PFF correction could also be improved by reducing the relative energy jitter (σ_p) or by increasing the upstream phase-energy correlation (ρ_{up}). Reducing the relative energy jitter decreases the additional phase jitter created by non-zero R56. Increasing the upstream phase-energy correlation (ρ_{up}) reduces the effect that non-zero R56 has on the upstream-downstream phase correlation (ρ_{ud}). For example, if $\rho_{up} = 1$ the source of all upstream phase jitter is energy jitter. In that case although non-zero R56 would further increase the downstream phase jitter, the additional jitter would be well correlated with the upstream phase and the upstream-downstream phase correlation would not be affected. In practice σ_p and ρ_{up} are defined by the CTF3 injector and can not be varied with a great degree of flexibility, so having zero R56 is the only way to obtain ideal conditions for the PFF correction. High upstream phase-energy correlations can be created at CTF3 but not without greatly amplifying the upstream phase jitter, which causes issues for the PFF system due to its limited correction range (Section 9.1).

An interesting side note of Equations 5.2 and 5.10 is that the best beam conditions for the PFF correction are not given by minimising the initial downstream phase jitter in the case where the upstream phase-energy correlation, ρ_{up} , is non-zero. As seen in the previous section in normal conditions there is a small correlation between the upstream phase and the energy at CTF3, typically around $\rho_{up} = 0.2$. In these conditions the downstream phase jitter can in theory be reduced to below the level of the upstream phase jitter by using a negative R56 to remove the energy component in the downstream phase. Differentiating Equation 5.2 gives the minimum downstream phase jitter to be obtained when $R_{56} = -\rho_{up}\sigma_u/\sigma_p$. However, using this R_{56} value would degrade the upstream-downstream phase correlation and increase the achievable corrected downstream jitter, which is always minimised when $R_{56} = 0$ as in Equation 5.10. This is significant for the R_{56} optimisation attempts presented later in this chapter, as it must always be kept in mind that the goal is to maximise the upstream-downstream phase correlation rather than to create the most stable downstream phase (with the PFF system off).

| Parameter | Value |
|-------------|-------------|
| R_{56} | -0.2 m |
| σ_u | 0.8° |
| ρ_{up} | 0.2 |
| σ_p | 0.001 |

Table 1.1: Typical upstream phase and energy conditions at CTF3.

1.3.3 Effect of R56 in TL2

Unfortunately, it was not possible to find optics for the TL2 chicane that met all the PFF requirements and thus an R56 in the chicane of close to -0.2 m had to be accepted (Section 3.4.3). All other lines at CTF3 nominally have zero R56 [REF], and therefore don't introduce additional phase jitter via energy, at least to first order and to within the accuracy of the CTF3 MADX model. The overall R56 between the upstream phase monitors (in the CT line) and the downstream phase monitors (in the TBL line, labelled CB, after the TL2 chicane) is therefore -0.2 m also. Whether this can explain the low upstream-downstream phase correlation and high downstream phase jitter seen in Section 5.2, as well as what residual R56 between the two monitors can be tolerated to be able to achieve CLIC-level phase stability at CTF3, is discussed in this section.

Equations 5.2 and 5.8 can be used to estimate the downstream phase jitter and upstream-downstream phase correlation in the conditions at CTF3. Typical values for the various parameters in the equations have already been presented in previous sections, and these values are summarised in Table 5.1. The value $R_{56} \simeq -0.2$ was obtained in Section 3.4.3 as previously mentioned, the value $\sigma_u \simeq 0.8^\circ$ in Section 5.2 and the values $\rho_{up} \simeq 0.2$ and $\sigma_p \simeq 0.001$ in Section 5.3.1.

With these parameter values the residual R56 of -0.2 m reduces the upstream-downstream phase correlation to below 10% [TODO: 45% on the other side of the crest, and there is ambiguity], and amplifies the downstream phase jitter to above 3 degrees. R56 transforming energy jitter in to downstream phase jitter therefore explains the low upstream-downstream phase correlation and high downstream phase jitter seen in Section 5.2. In order to increase the upstream-downstream phase correlation to 97% and reduce the downstream jitter to 0.8 degrees (the conditions needed to achieve 0.2 degrees corrected downstream phase jitter at CTF3, see Section 2.5) the R56 between the upstream and downstream phase monitors must be removed.

Figure 5.1 and 5.2 show the expected downstream phase jitter and upstream-downstream phase correlation for residual R56 values from -0.2 to +0.2 m between the upstream and downstream phase monitors again using the equations derived in the previous section. The horizontal black line in each figure marks the requirements needed to reduce an initial upstream phase jitter of 0.8 degrees to the CLIC target of 0.2 degrees. The red line, "corrected", in Figure 5.1 shows the theoretical corrected downstream phase jitter using the PFF correction across the range of R56 values. Note the slight asymmetry in the phase jitter and correlation curves, which is caused by the non-zero correlation between the upstream phase

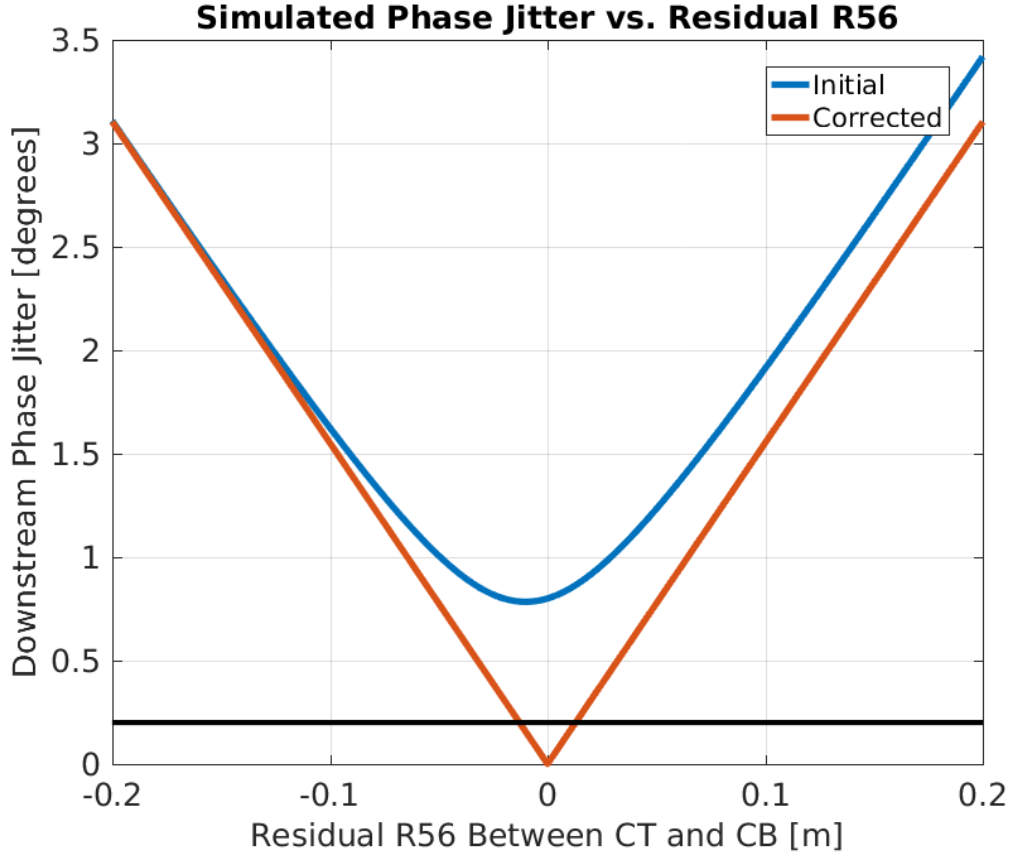


Figure 1.1: Downstream phase jitter vs. residual R56 between monitors.

and the beam energy. In order to obtain CLIC level phase stability at CTF3 the residual R56 between the upstream and downstream phase monitors must be reduced from the initial $-0.2m$ to $0 \pm 1.3 \text{ cm}$.

To interpret the results of the R56 optimisation attempts presented in the remainder of this chapter it is useful to understand how varying the correlation between the upstream phase and the energy (ρ_{up} changes the dependence of the upstream-downstream phase correlation (ρ_{ud}) on the residual R56. In particular, in Section 5.5.3 a machine setup that increases ρ_{up} to 90% was used. Figure 5.3 shows how ρ_{ud} varies with ρ_{up} values between 0% and 40% (typical of normal operation) and with the higher correlation of 90%. With high correlations between the upstream phase and energy there is no longer a well defined peak in ρ_{ud} versus the residual R56 value. Instead there is an almost constant high upstream-downstream phase correlation with positive R56 values, and a large anti-correlation for negative R56 values (as in this case the residual R56 acts to flip the sign of the phase jitter).

In Figure 5.4 plotting the theoretical downstream jitter with $\rho_{up} = 0.9$ gives a clear demonstration that the best conditions for the PFF correction are always with $R_{56} = 0$ rather than with the lowest possible initial downstream jitter, as mentioned in the previous section. In fact, as these conditions relax the requirements on the residual R56 needed to achieve high upstream-downstream phase correlations (as seen in the previous figure) it may be easier to achieve a large factor reduction in the downstream phase jitter with the

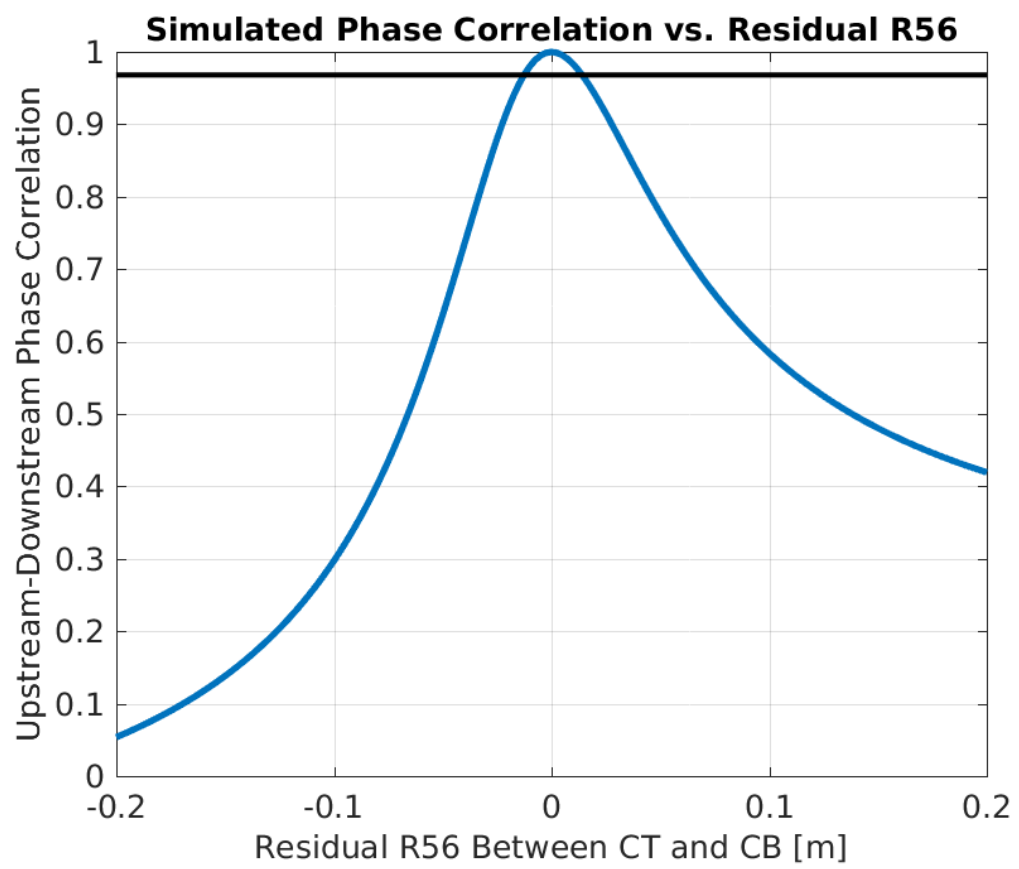


Figure 1.2: Phase correlation vs. residual R56 between monitors.

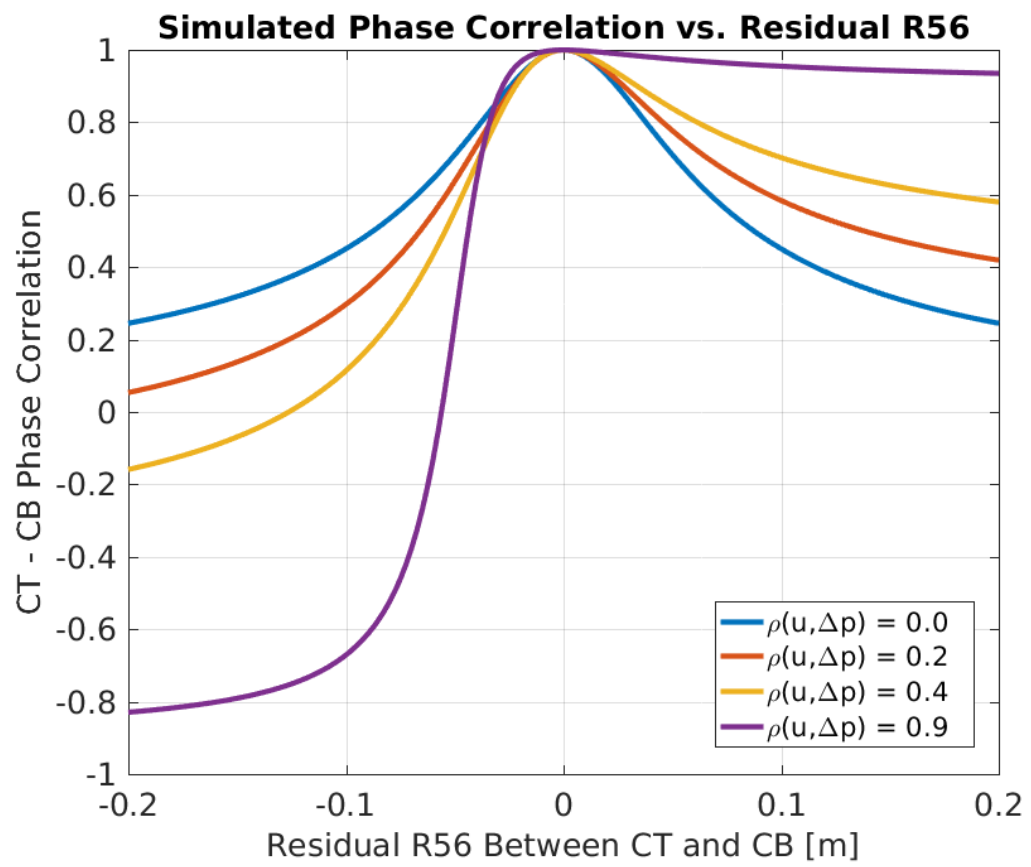


Figure 1.3: Phase correlation vs. residual R56 between monitors.

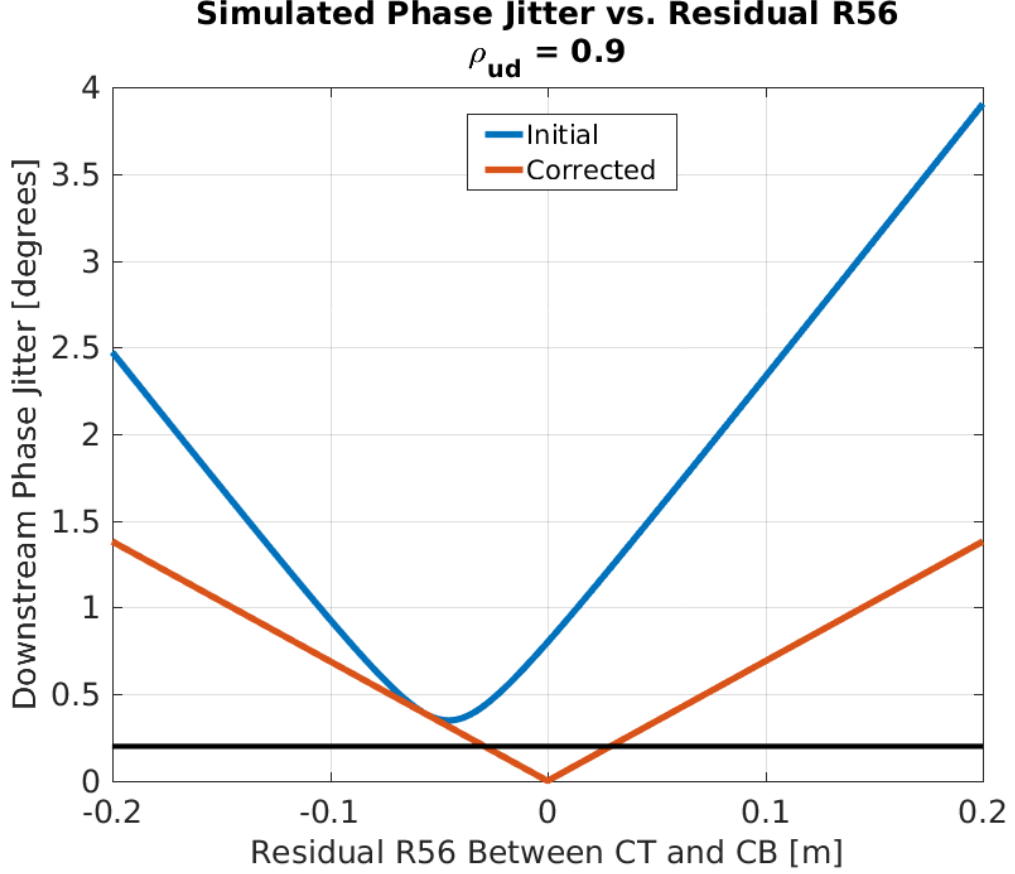


Figure 1.4: Phase correlation vs. residual R56 between monitors.

PFF system with a high ρ_{up} machine setup. This has been attempted and is presented in Section 9.1.

1.4 Mitigation of First Order Energy Dependence

The discussion in the previous section proves that with a residual R56 value of -0.2 m between the upstream and downstream phase monitors it is impossible to achieve the goals of the PFF prototype at CTF3. However, due to the highly constrained optics in TL2 it has already been seen in Chapter 3 that it was not possible to find optics for the PFF chicane that yield zero R56 whilst also meeting requirements for both the PFF system and transverse matching (dispersion and beta functions). The only way to create a total R56 of zero between the upstream and downstream phase monitors is therefore to add positive R56 to one of the other beam lines at CTF3 in order to compensate for the negative R56 in the TL2 chicane.

The previous transfer line TL1, which transports the beam from the CT line (where the upstream phase monitors are installed) to the combiner ring (see Figure 2.1), has been used to achieve this. The layout of the TL1 transfer line is shown in Figure 5.5. It consists of: 4 dipoles (bending the beam horizontally) of 2 different types, 13 quadrupoles of 5 different types, 7 magnetic correctors, 1 sextupole (usually not used) and 8 BPMs (the dispersive

BPM after the first dipole in TL1, labelled CT.BPI0608, is the device that has been used to determine correlations between the phase and energy in this chapter). The total length of TL1 is approximately 30 m. [TODO: more details?]

Preliminary attempts to reduce the residual R56 between the upstream and downstream phase monitors using TL1 yielded correlations up to 60% and reduced the downstream phase jitter to 2° . Conditions similar to these were used for the first PFF tests (Chapter 7) before the energy related effects discussed in this chapter were fully characterised, but in these tests only a modest reduction of 30% in downstream phase jitter was possible due to the limitations of the phase propagation shown here. At this time only a few different optics for TL1 were available in R56 steps of 10 cm. As the total residual R56 must be reduced to the centimetre level to make a correction down to 0.2 degrees jitter theoretically possible with the PFF system, new sets of optics for TL1 were required.

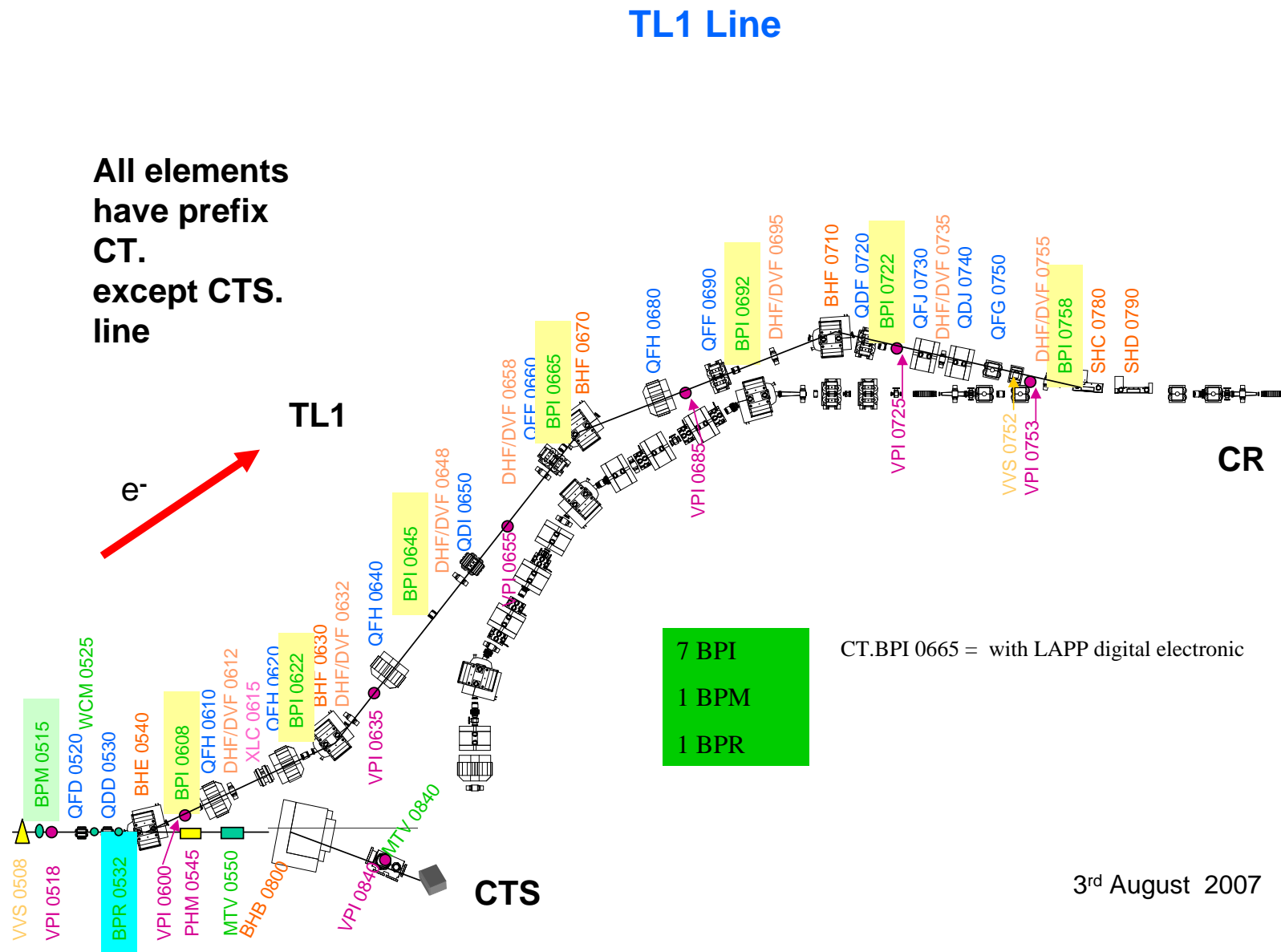


Figure 1.5: TL1 [REF].

| Parameter | TL1 Injection | CR Injection |
|------------|---------------|--------------|
| β_x | 8.81 m | 4.08 m |
| β_y | 13.94 m | 5.41 m |
| α_x | -0.74 | -0.31 |
| α_y | -0.45 | -0.21 |
| D_x | 0 m | -0.03 m |
| D_{px} | 0 | 0.02 |

Table 1.2: Initial and final conditions for optics matching in TL1.

[TODO: Need a better figure]

1.4.1 Matched Optics for TL1

Although in theory only one set of optics with $R_{56} = +0.2$ m in TL1 is required to compensate for the $R_{56} = -0.2$ m in TL2, in practice errors in the MADX model of CTF3 plus the effect of higher order energy dependencies (see Section 5.5) means it is not possible to know precisely what the optimal R56 to set in TL1 will be, and it is also possible that this value will vary with time. To determine the optimal value of R56 to set it is also useful to scan the R56 value in TL1 across a wide range of values and then fit the maximum resulting upstream-downstream phase correlation.

To allow this, MADX has been used to match optics for TL1 with R56 values ranging from -0.3 m to +0.6 m in steps of 0.5 cm (a total of 181 sets of optics). The optimal R56 value should always be guaranteed to be in this range, and the step size of 0.5 cm allows the residual R56 to be zeroed to within one centimetre as derived to be necessary in Section 5.3.3. As well as the different R56 values, each set of optics must maintain the same initial and final conditions, so that the injection of the beam in to the combiner ring is not affected. Values for the beta functions, alphas and dispersion at the start of TL1 and at the combiner ring injection are summarised in Table 5.2. As well as the initial and final conditions, the maximum beta functions and dispersion in TL1 are constrained to ensure a reasonable beam size throughout the line — the horizontal and vertical beta function is limited to a maximum of 35 m, and the horizontal dispersion to a maximum absolute value of 1.25 m. Around the septum used for injection in to the combiner ring the horizontal beta function is further limited to a maximum of 10 m. The strengths of the 13 quadrupoles in TL1 are varied to meet all these constraints.

Figures 5.6 shows the matched R56 value in TL1 across the range of targeted values. Each matched R56 value is within 10 microns of the desired result. Figure 5.7 then shows an example of how the strength of one of the quadrupoles must be varied in order to achieve each R56 value. If the dependence of each quadrupole strength on the R56 value was continuous the relationship could be fitted to create a set of tuning knobs to allow R56 to be set to any arbitrary value in TL1. However, as seen in the figure there are many discontinuities. The quadrupole strengths for each set of optics are therefore saved to a lookup table, with a MatLab function created to read the table and set the quadrupole currents in the machine

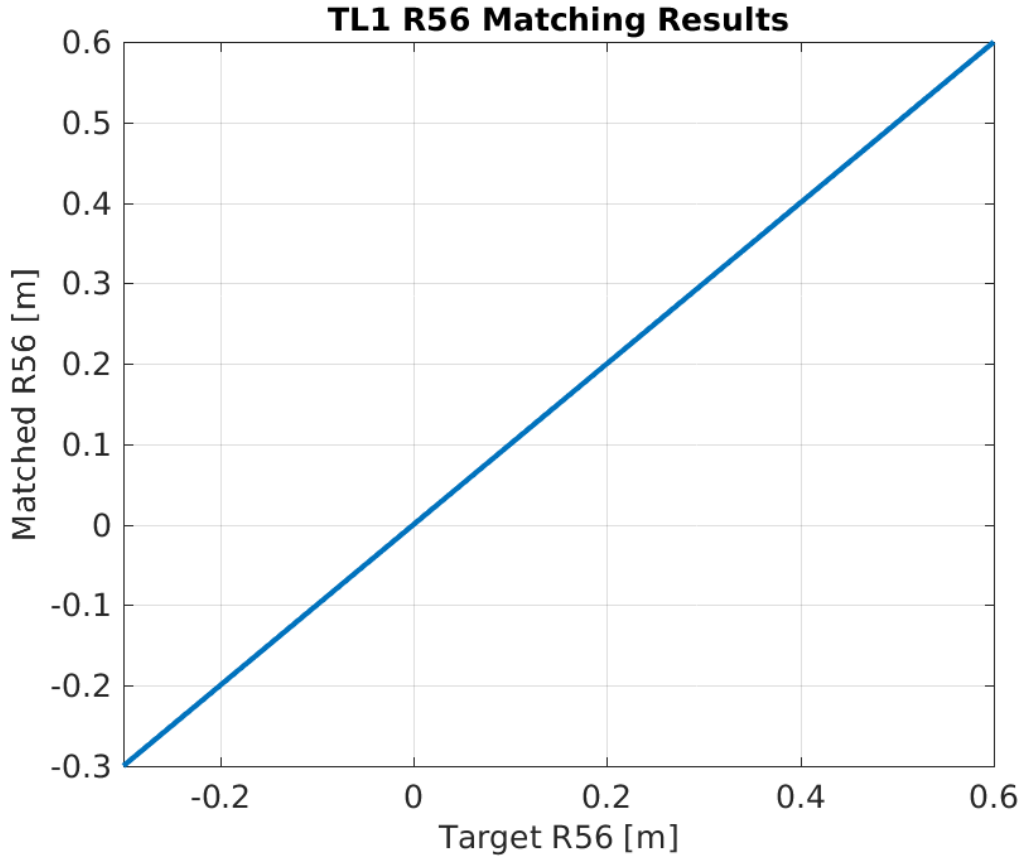


Figure 1.6: Matched R56 values for TL1.

appropriate for the specified R56 value. As already mentioned 0.5 cm precision in R56 should be adequate for the PFF requirements, but the discontinuities mean new optics would have to be matched if optics with an R56 value not included in the discrete set used here were required.

For reference Figures 5.8 5.9 and 5.10 show how the horizontal and vertical beta functions and horizontal dispersion changes in TL1 for each set of optics. For all R56 values each parameter converges to the same value at the start and end of TL1, as needed to ensure that changing the R56 does not impact injection in to the combiner ring. The maximum horizontal and vertical beta functions in TL1 roughly increase with the set R56 value, but in all cases are kept below the set limit of 35 m in the matching procedure. The dispersion pattern in TL1 also changes with the set R56 value, though in most cases the maximum absolute dispersion is around 1 m and only the location of the peak dispersion along the line changes. Again, for each set of optics the maximum absolute dispersion is limited within the set constraint of 1.25 m.

Commissioning of the new TL1 optics in CTF3 was straightforward and in general they can be set with the quadrupole strengths at their nominal matched values without causing issues for the beam quality. At the extremities of the range of optics (close to $R56 = -0.1$ m and $R56 = +0.6$ m) some slight beam losses do begin to occur, but this is not a problem for PFF operation where the required R56 is only 0.2 m. However, for each set of optics the

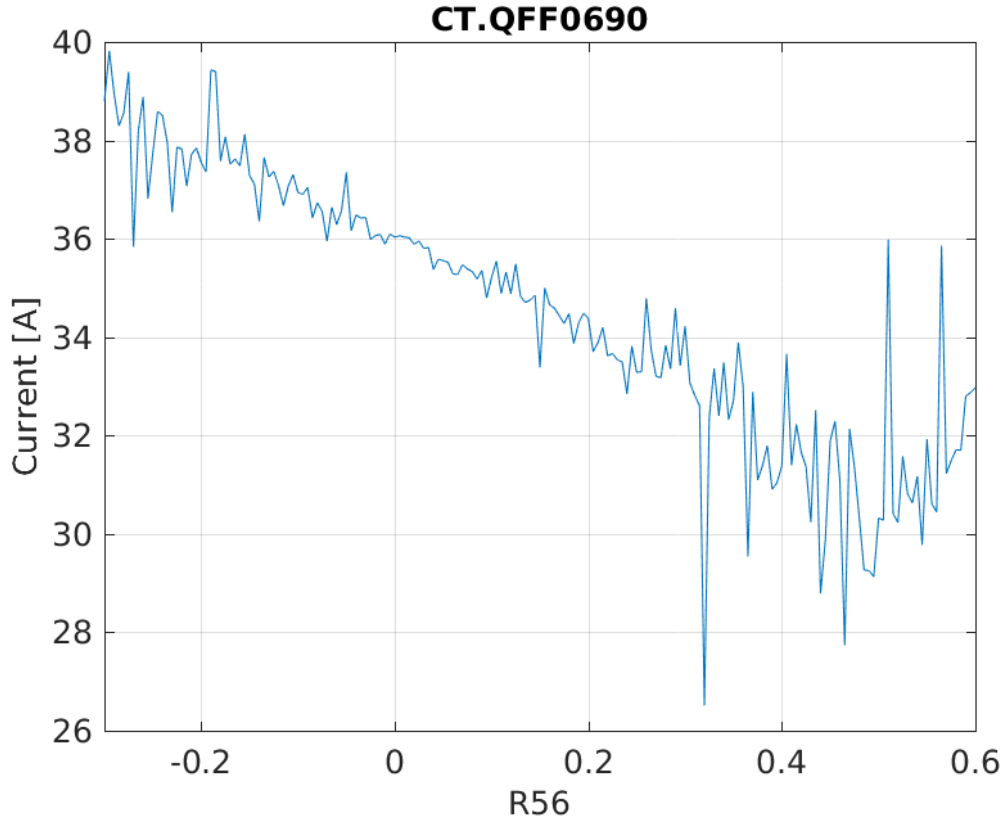


Figure 1.7: Current vs. R56 for the CT.QFG0750 quadrupole in TL1.

magnetic correctors in TL1 may need to be changed to recover the nominal beam orbit, thus taking in to account slight misalignments in elements along the line. [TODO: could expand this]

1.4.2 Scans of R56 in TL1

The sets of matched optics from the previous section can be used to perform scans of the R56 value in TL1 to observe how the downstream phase is affected. Scans of this type must be performed prior to all PFF data taking periods in order to optimise the beam conditions (maximise the upstream-downstream phase correlation) for the correction. More recently scans of R56 in TL1 have been performed whilst varying the beam energy, which produces cleaner results and highlights additional factors that must be taken in to account during the optimisation process, as will be shown in Section 5.5.

As a starting point the simplest case, where only the TL1 optics is changed during the scan and all other parameters in the machine are left unchanged, is presented in this section. This also highlights some of the difficulties in maintaining beam conditions at CTF3, which is discussed further in Section 5.5 and extensively in the context of the PFF correction in Section 8.2. Figures 5.11 and 5.12 show one example of an R56 scan performed across the full range of available optics – from -0.1 m R56 in TL1 to +0.6 m. The R56 is incremented by 2.5 cm between datasets, to give a total of 29 R56 points in the scan, with the whole scan

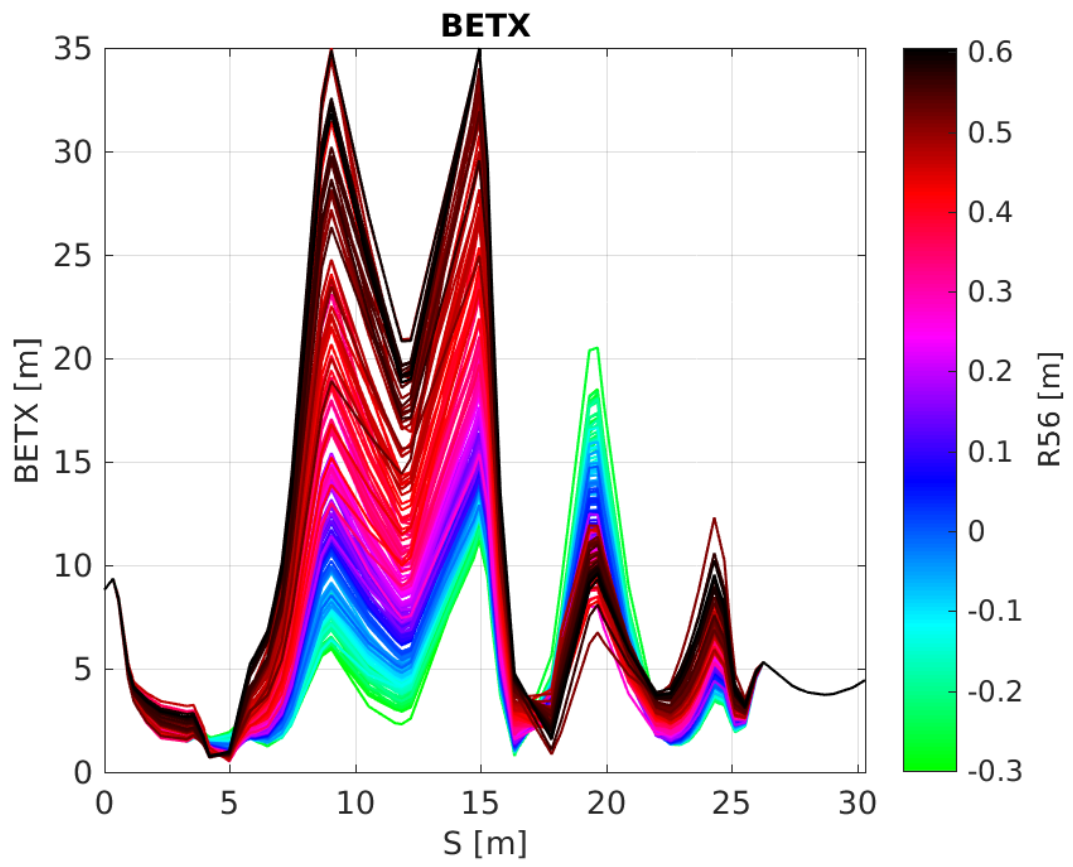


Figure 1.8: Horizontal beta in TL1 for all R56 optics.

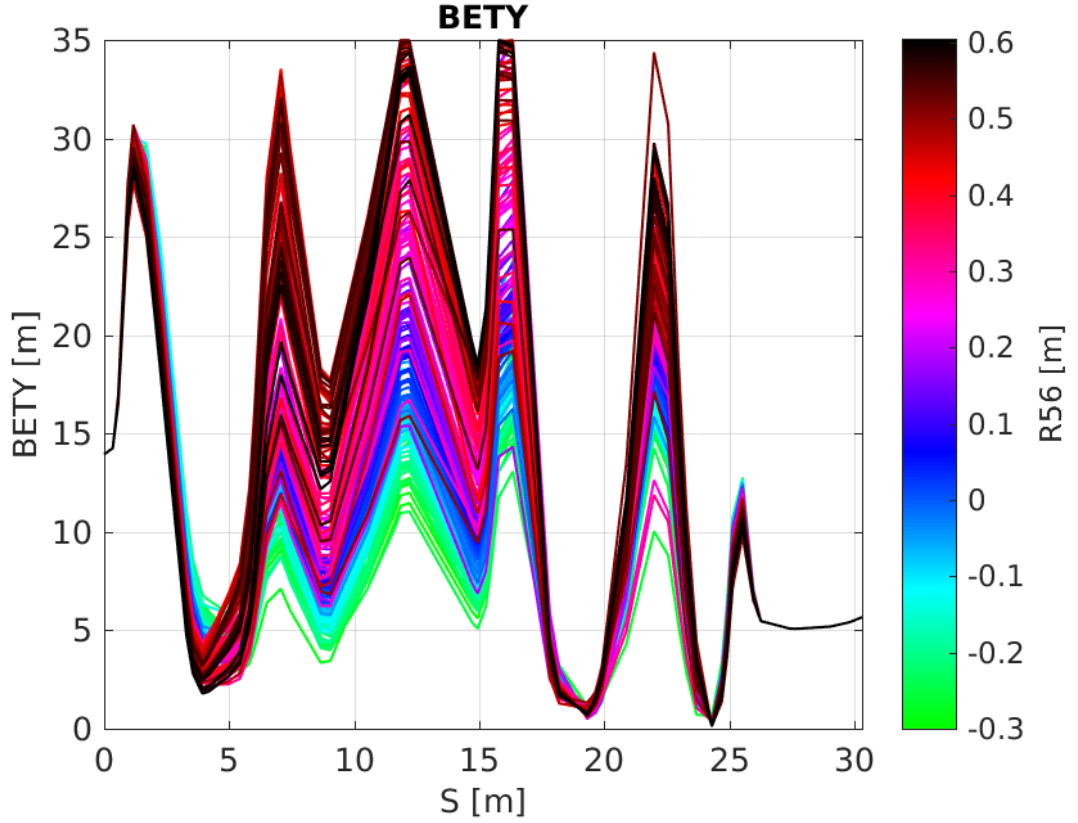


Figure 1.9: Vertical beta in TL1 for all R56 optics.

taking approximately one and a half hours to complete. With the knowledge gained from measurements of this type it is no longer necessary to scan the R56 across the full range to determine the ideal value, thus the optimisation of the phase propagation for PFF attempts can now be achieved on much shorter time scales.

Mean Phase

Only the mean phase jitters and correlation will be considered here, features along the pulse are discussed in later sections for other scans. Figure 5.11 shows the mean phase jitter during the scan both upstream and downstream. Although the noise in the measurement is quite large, the downstream phase jitter is reduced from above 2.5 degrees with zero R56 in TL1, to below 1 degree and close to the level of the upstream phase jitter by adding positive R56 in TL1. The optimal R56 value is approximately 0.175 m, in close agreement with expectations considering the -0.2 m R56 in TL2. The upstream-downstream phase correlation, in Figure 5.12, is also maximised at this point, from an initial correlation of 20% with zero R56 to up to 80%. In terms of the PFF system, increasing the upstream-downstream phase correlation from 20% to 80% improves the theoretical correction from a 2% reduction in downstream phase jitter to a 40% decrease (Equation 2.1).

As the upstream phase monitors are prior to TL1, changing the TL1 optics has no effect on the upstream phase jitter. All differences in the upstream phase jitter between datasets

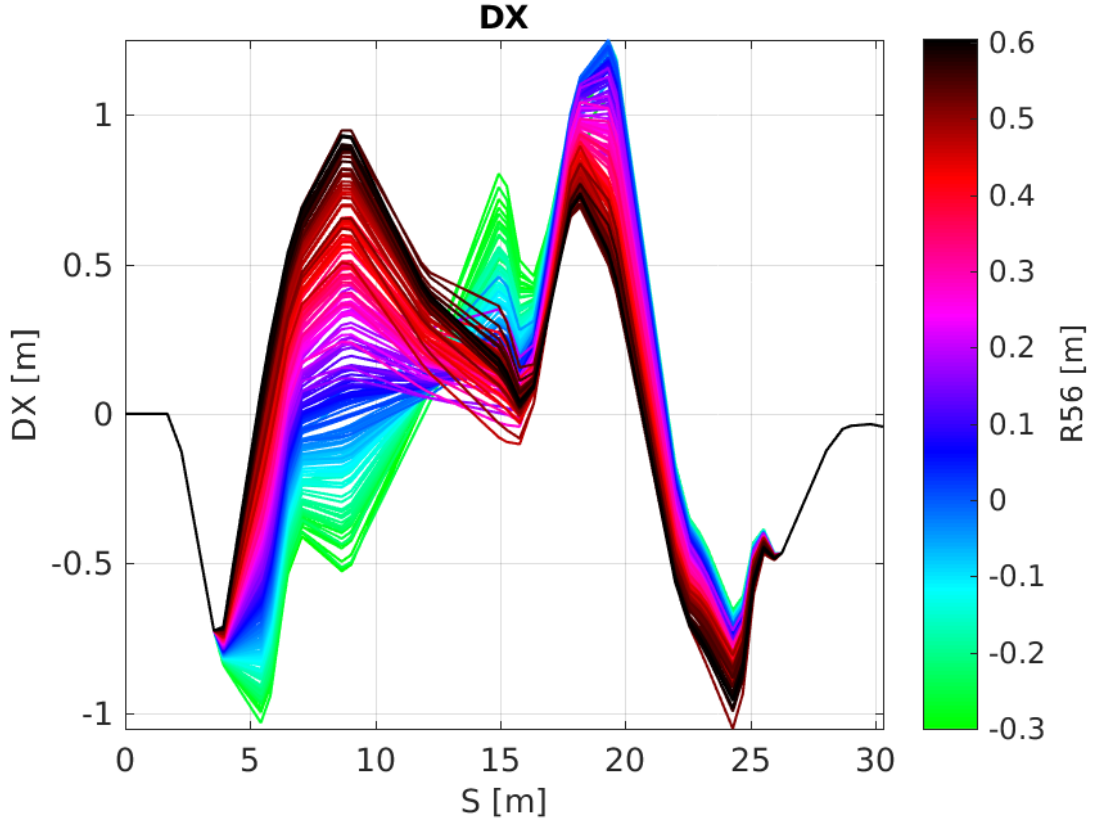


Figure 1.10: Dispersion in TL1 for all R56 optics.

are caused by drifts in the CTF3 injector, typically changes in either klystron phases or beam current. Although the overall stability of the upstream phase jitter during this scan is good, it does vary between 0.5 degrees and 1.2 degrees. In addition to the upstream phase there are also differences in the relative energy jitter and upstream phase-energy correlation during the scan, as seen in Figure 5.13. The relative beam energy jitter varies between 0.4×10^{-3} and 1.0×10^{-3} and the upstream phase-energy correlation between -0.5 and +0.5. All these parameters influence the downstream phase, as per the equations in Section 5.3.2.

The differences in the upstream phase and energy conditions between datasets partially explains the apparent spread of the data points away from the expected clean distribution. The black “simulation” lines in Figures 5.11 and 5.12 represent the expected downstream phase jitter and upstream-downstream phase correlation at each point in the scan given the upstream phase jitter, relative energy jitter and upstream phase-energy correlation at that time (using Equations 5.2 and 5.8). The correlation simulation in Figure 5.12 has been scaled so that the peak value is in agreement with the data, at 0.8. The majority of the data points follow the scaled simulated distribution, with several remaining outliers. For the downstream phase jitter (which uses the simulated result directly with no scaling) the agreement with the simulation is generally good for R56 values below 0.3 m. However, above 0.3 m the actual phase jitter seen in the scan is smaller than the simulation. One possible explanation for this are the changes in downstream beam current between datasets, which varies by a factor 3 during the scan (bottom plot in Figure 5.13). Small beam losses between measurements may change the phase jitter in a way that is not characterised by the R56.

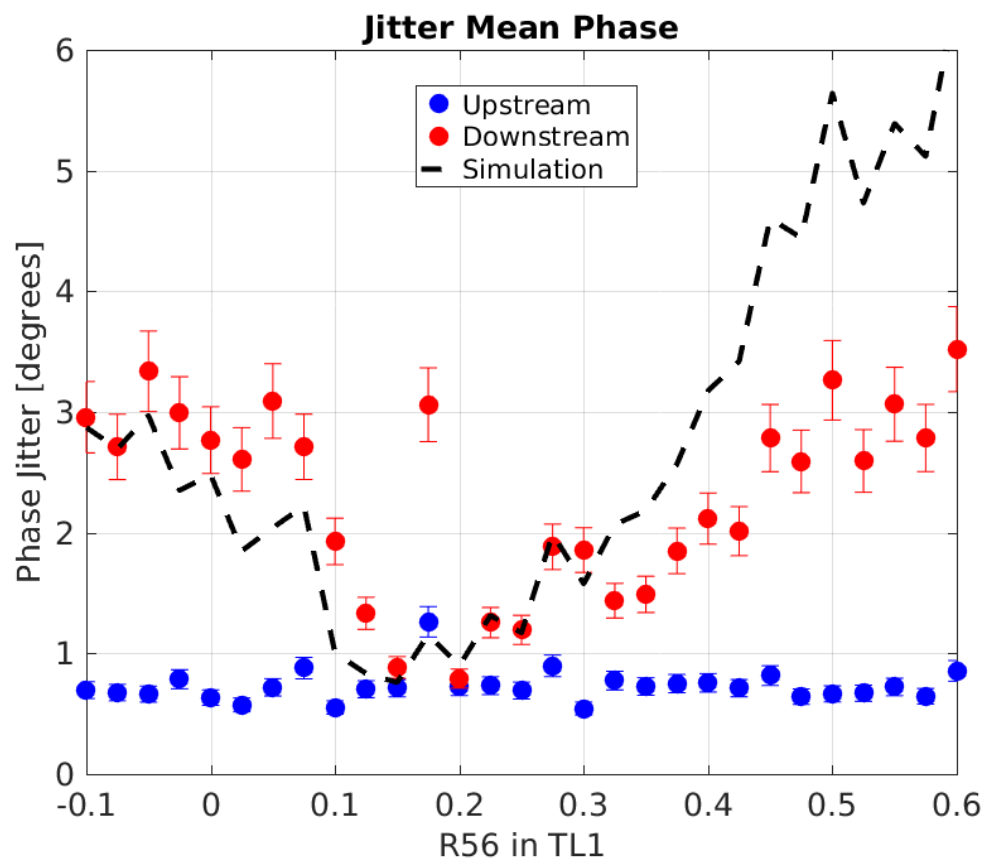


Figure 1.11: Phase jitter during scan of R56 in TL1.

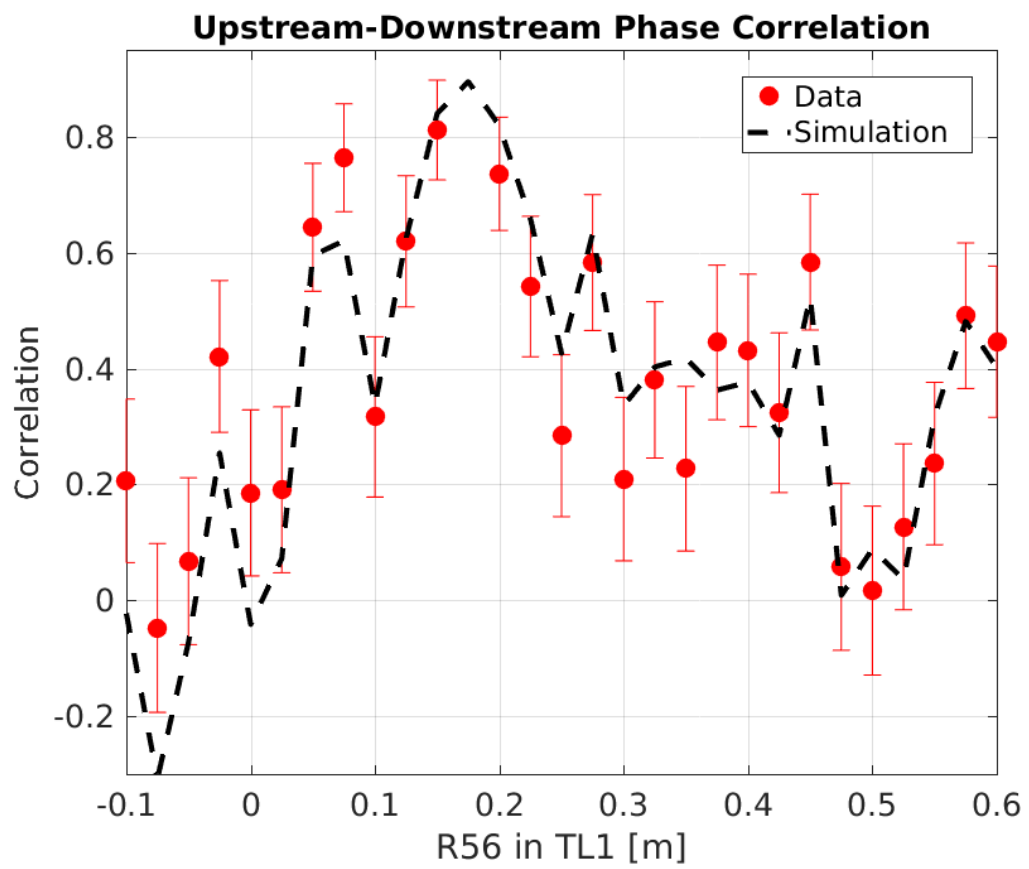


Figure 1.12: Correlation during scan of R56 in TL1.

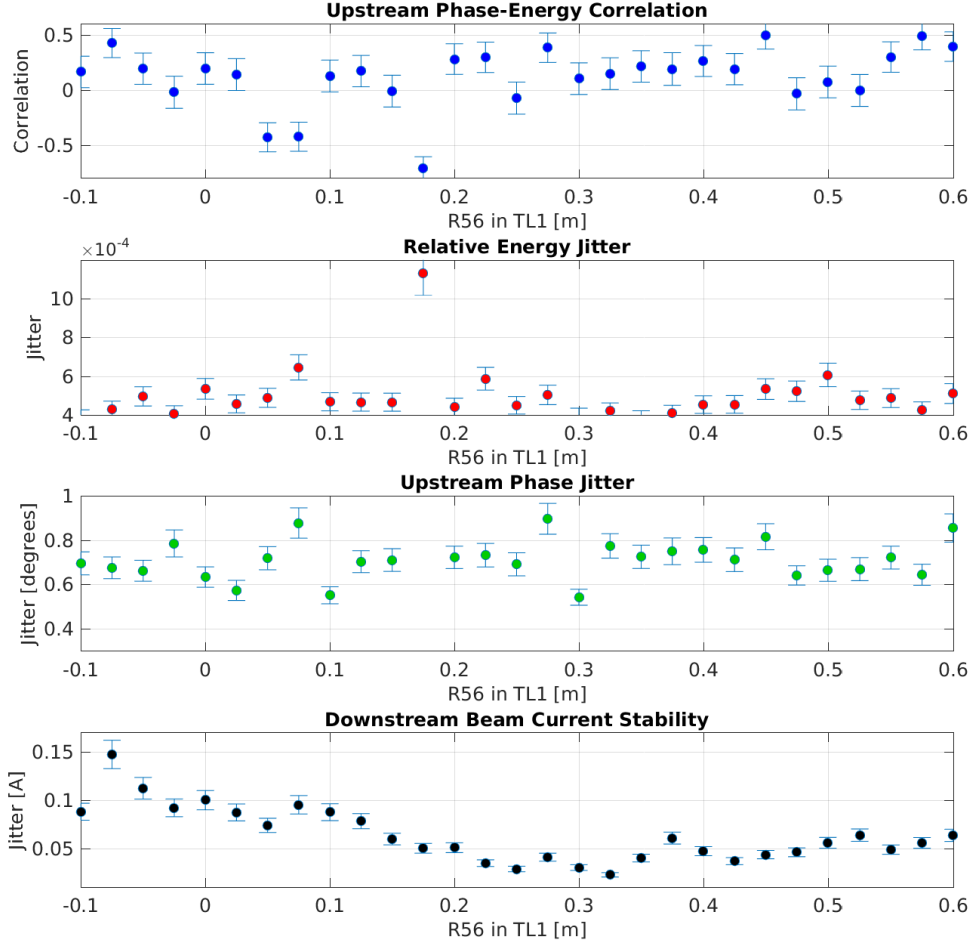


Figure 1.13: Upstream and downstream beam conditions during the R56 scan.

Possible other sources are discussed in Sections 5.5 and 5.6.

Results from Other Scans

Figures 5.14 and 5.15 show the results of two further scans of R56 in TL1, both taken a few days after the scan previously shown. For both scans the mean downstream phase jitter can again be decreased to the level of the upstream phase jitter by varying the R56 in TL1, and the upstream-downstream correlation increased to 80%. However, the optimal optics to use is different for each scan — the scan in Figure 5.14 has an optimal R56 value of around 0.1 m whereas for the scan in Figure 5.15 the optimal value quite close to zero, around 0.04 m. Both values are also different to the scan previously shown, which had an optimal R56 setting of 0.175 m.

With R56 alone and the model of the phase propagation used to derive the equations in Section 5.3.2 there is no mechanism for the optimal R56 value to vary with time. The best conditions for the phase propagation should always be provided with zero residual R56

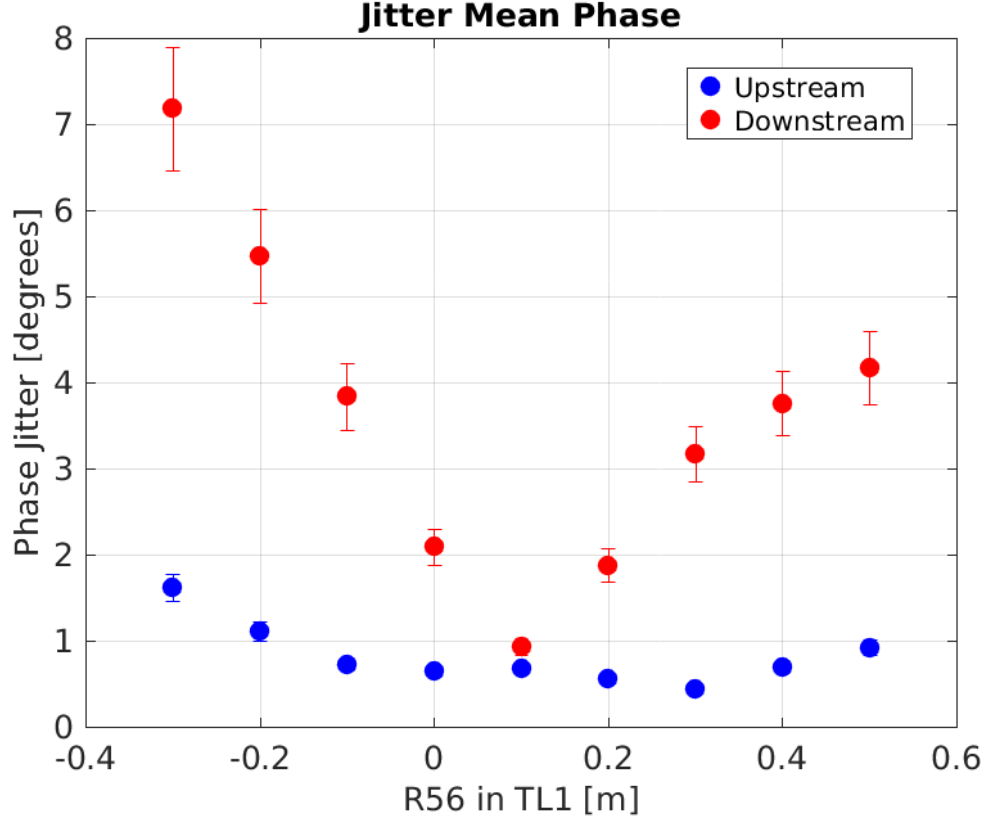


Figure 1.14: Mean phase jitter during R56 scan 2.

between the upstream and downstream phase monitors. As the optics in all beam lines between the upstream and downstream phase monitors (apart from TL1) were unchanged between each scan, the optimal R56 value in TL1 should also be the same for each scan in this model. The most likely explanation is a sensitivity to higher order energy dependencies.

1.5 Higher Order Energy Dependencies

1.5.1 Expected Dependence due to Optics

In the same way the first order optics dependencies are described by the 6×6 R-matrix, the second order effects are described using a three dimensional $6 \times 6 \times 6$ T-matrix. R_{56} is the relevant first order transfer matrix coefficient for the energy related effects on the phase propagation, as already discussed, and it then follows that the relevant T-matrix coefficient for second order energy dependencies is T_{566} . By including the second order term the dependence of the downstream phase on the energy from Equation 5.1 becomes:

$$\phi_d = \phi_u + R_{56} \frac{\Delta p}{p} + T_{566} \left(\frac{\Delta p}{p} \right)^2 \quad (1.11)$$

$$\phi_d = \phi_u$$

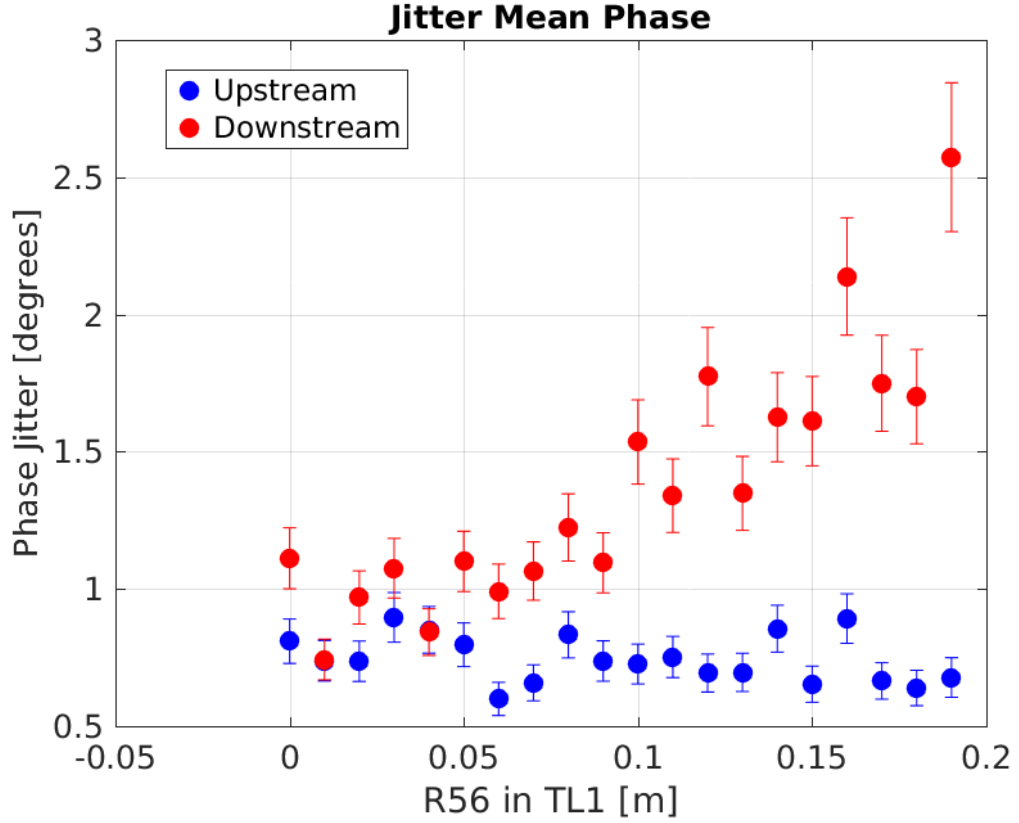


Figure 1.15: Mean phase jitter during R56 scan 3.

$$R_{56} = -T_{566} \frac{\Delta p}{p} \quad (1.12)$$

1.5.2 Energy Variation Along the Pulse

and different R56 optimal point along pulse

1.5.3 R56 Scans whilst Varying Beam Energy

Phase Along the Pulse

As well as the mean phase it is interesting to look at the effect of varying the R56 on the phase along the pulse. Figure 5.18 shows the mean phase along the pulse for each R56 setting in TL1 during the scan. Any difference in the mean (rather than the jitter) along the pulse with the R56 value should originate from static energy variations along the pulse. If the energy along the pulse was constant changing the R56 would only affect the phase jitter and would not change the mean pulse shape. The clear change in certain features along the pulse in the downstream phase is therefore an indication of energy variations in these regions. Perhaps the best example of this is the oscillation around a time of 800 ns,

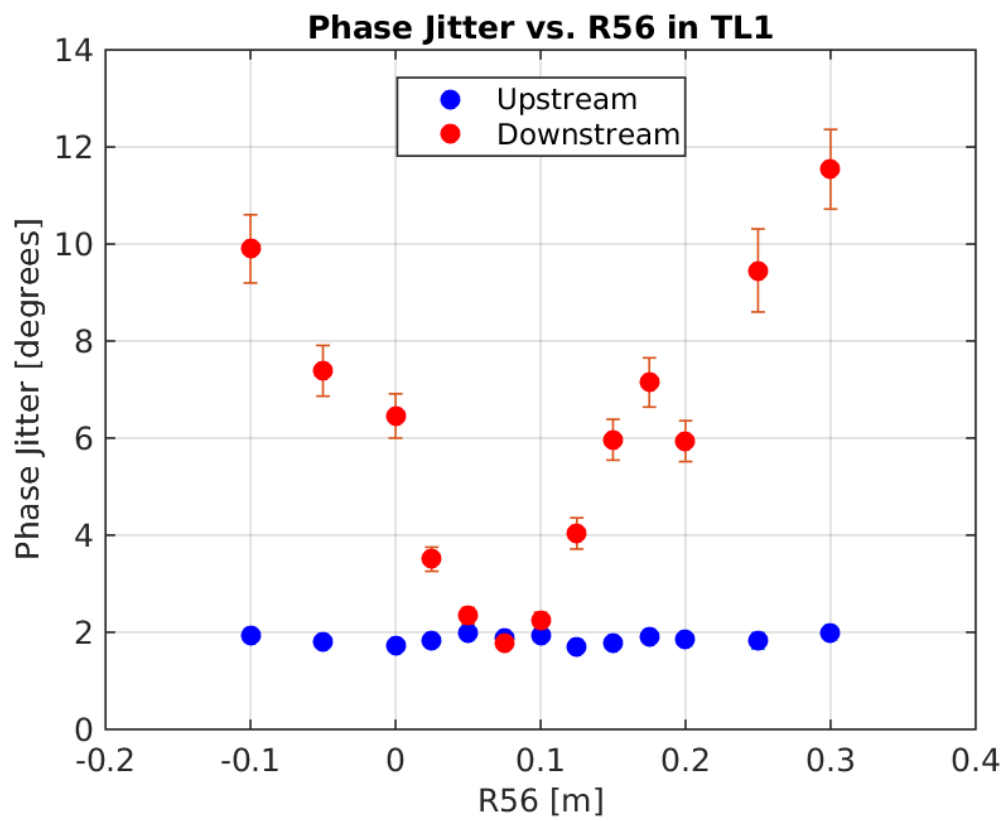


Figure 1.16: Phase jitter for different R56 whilst wiggling gun current.

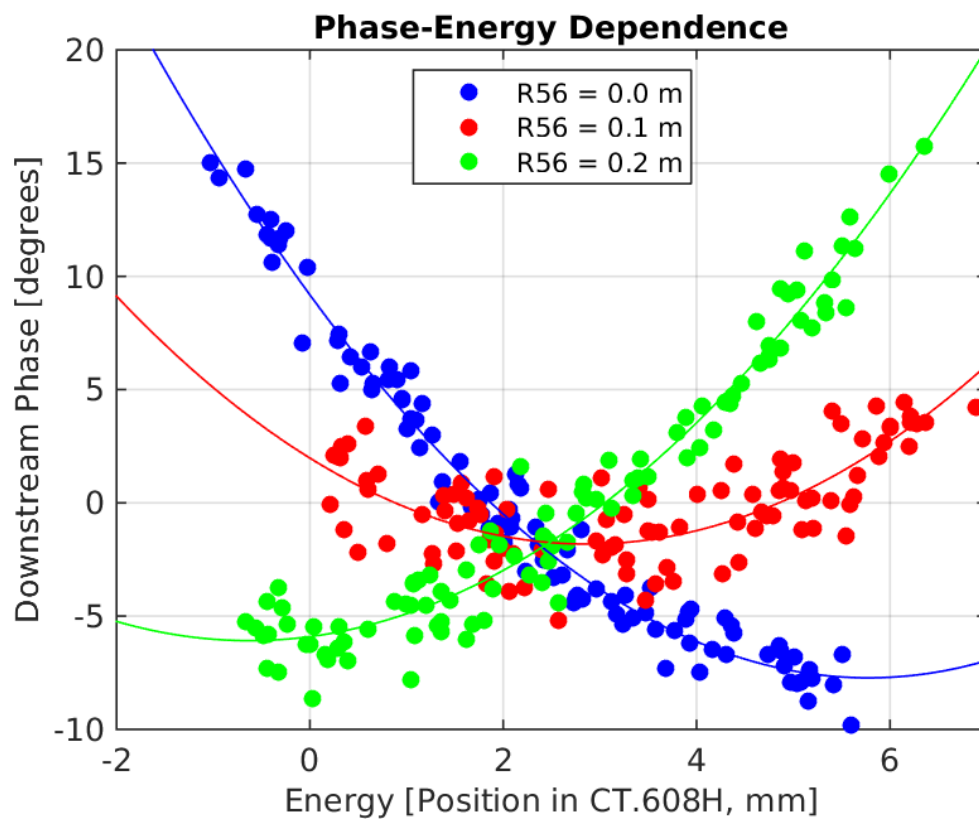


Figure 1.17: Phase vs. energy for different R56 in TL1.

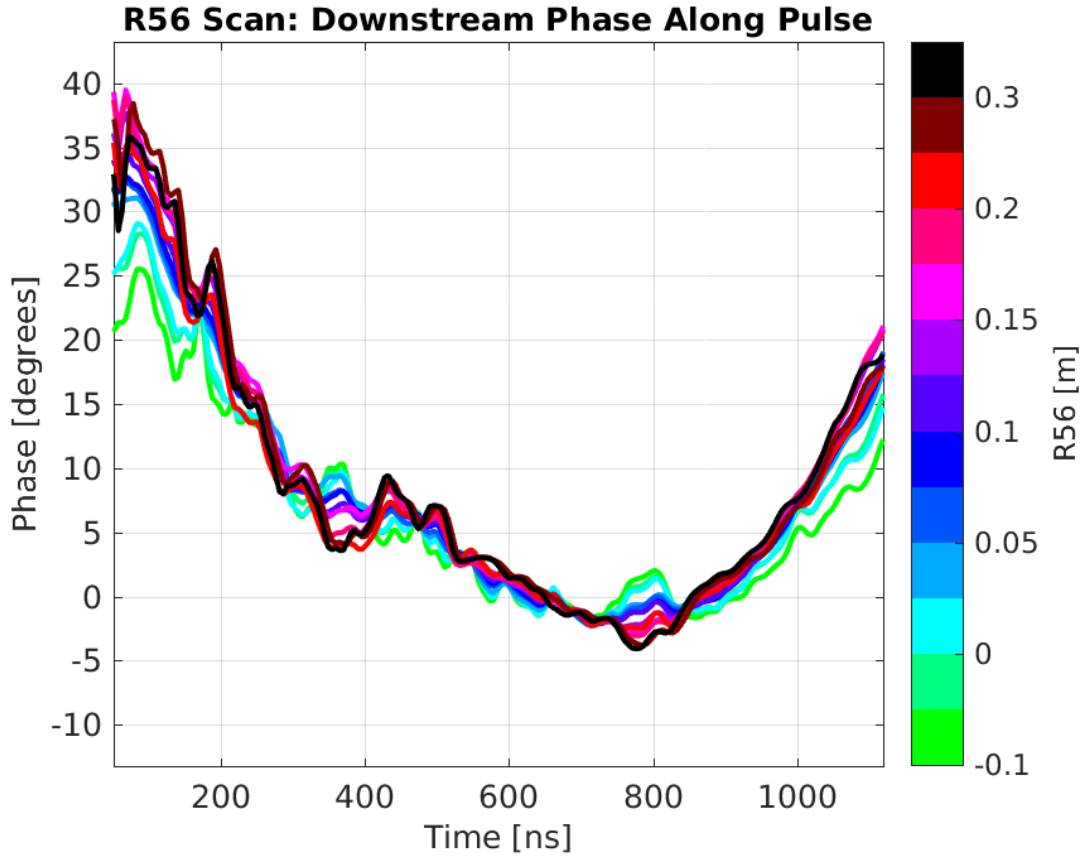


Figure 1.18: Mean downstream phase along the pulse for different R56 values.

where the phase is flat close to the optimal R56 value of 0.175 m but swings upwards when a negative R56 in TL1 is used or downwards for R56 values above 0.175 m.

The difference between the phase along the pulse for two different settings of R56 in TL1 should be proportional to the beam energy along the pulse. Figure 5.19 plots the difference between the R56 = +0.3 m optics and the optimal R56 = +0.175 m optics, and compares this to the beam energy along the pulse (measured using the horizontal beam position in the dispersive BPM after the first dipole in TL1). Both lines are mean subtracted and normalised to give equivalent amplitudes in arbitrary units. For reference the peak to peak beam position offset along the pulse is 1.6 mm in this case, corresponding to a relative energy offset along the pulse of 2.3×10^{-3} . Overall, the differences in phase along the pulse resulting from using non-optimal R56 in TL1 are very well matched with the energy variation along the pulse, as expected.

[TODO: comparison of upstream and downstream phase along the pulse]

[TODO: Jitter along the pulse]

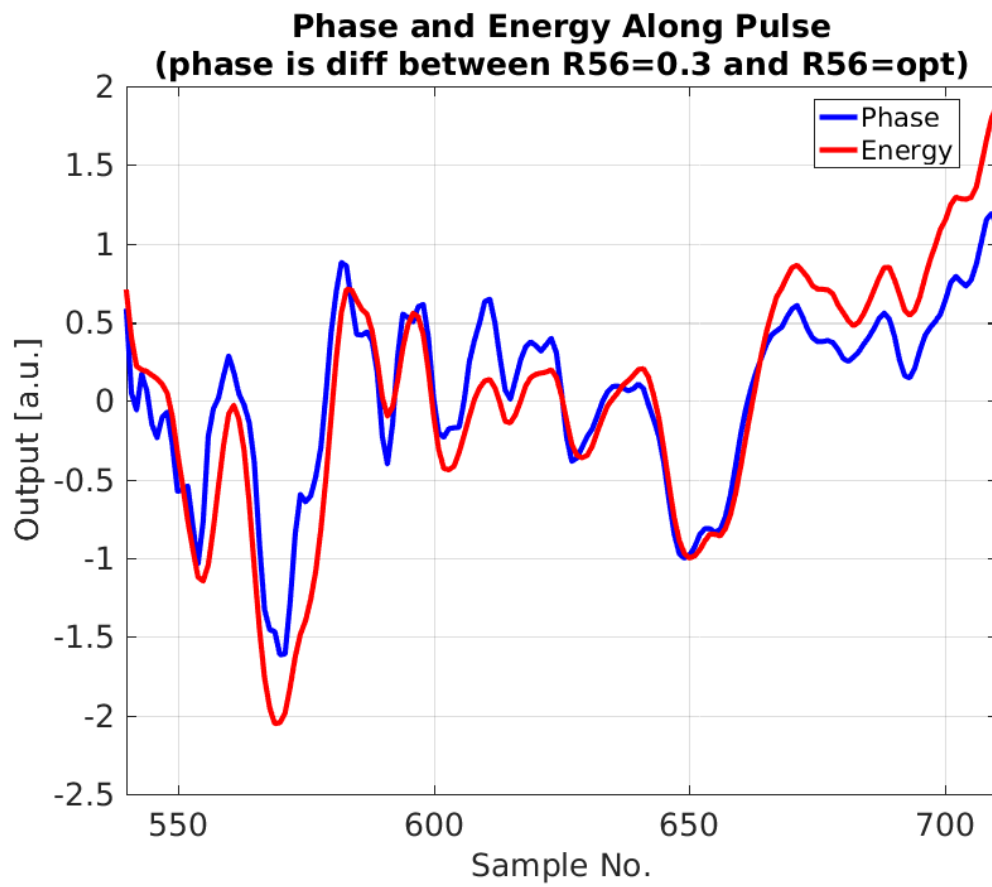


Figure 1.19: Mean downstream phase along the pulse for different R56 values.

1.5.4 Mitigation of Higher Order Dependencies

1.5.5 Effect on PFF Operation

1.6 Other Sources of Phase Jitter

1.6.1 Combiner Ring Septum

1.6.2 TL1 & Combiner Ring Bends

RF Deflector

CR Septum

TL1/CR Bends

1.7 Best Phase Propagation

some kind of drift analysis of drift sources to be able to refer back to it in long PFF results section

Bibliography

- [1] Dummy One & Dummy Two. *Phys. Journal*, **1**, 1 (2002) 1–5. hep-ph/0000000.
<http://some.web.address>